Actin cytoskeleton dynamics affect replication of Human Metapneumovirus

Pamela Elizabeth Rodríguez[a§], Pedro Ignacio Gil[b§], Jorge Augusto Cámara[a], Alicia Cámara[a] and María Gabriela Paglini*[b,c]

[a]Laboratory of Influenza and other Respiratory Viruses, Virology Institute "Dr. J. M. Vanella". Facultad de Ciencias Médicas. Universidad Nacional de Córdoba. Córdoba. Córdoba. Argentina.
[b]Laboratory of Cell Biology of Viral Infection, Virology Institute "Dr. J. M. Vanella". Facultad de Ciencias Médicas. Universidad Nacional de Córdoba. Córdoba. Córdoba. Argentina.
[c]Laboratory of Neurophysiology, Instituto de Investigación Médica Mercedes y Martín Ferreyra, INIMEC-CONICET, Universidad Nacional de Córdoba, Córdoba, Argentina.

§: Pamela Elizabeth Rodriguez and Pedro Ignacio Gil contributed equally to this work.

***Corresponding author.**
María Gabriela Paglini, Ph.D. ORCID: 0000-0002-2565-8699
Laboratory of Cell Biology of Viral Infection, Virology Institute "Dr. J. M. Vanella". Facultad de Ciencias Médicas. Universidad Nacional de Córdoba. Córdoba. Argentina,
Enfermera Gordillo s/n. Ciudad Universitaria, 5000 - Córdoba Argentina.
Phone: +54-351-4334022
E-mail: gpaglini@immf.uncor.edu

ORCID:
Pamela Elizabeth Rodríguez (rpamelaelizabeth@gmail.com): 0000-0003-3827-3760
Pedro Ignacio Gil (pedro.gil@unc.edu.ar): 0000-0002-5444-063X
Jorge Augusto Cámara (jcamara@fcm.unc.edu.ar): 0000-0002-5072-2795
Alicia Cámara (camaraalicia@yahoo.com.ar): 0000-0003-3988-2664

Word count manuscript: 3526

Word count abstract: 200

Author contribution

All authors were responsible for the study design. PER, PIG performed the experimental procedures and collected/curated data. PER and PIG conducted statistical data analysis. PER,

PIG, AC and MGP performed imaging analysis. JC, AC and MGP contributed ideas and comments. PER, PIG, JC, AC and MGP interpreted the findings and drafted the manuscript. Supervision and project administration were done by AC and MGP and funding's acquisition by MGP and AC. All authors have read and agreed to the published version of the manuscript.

Short title

Human Metapneumovirus replication dynamics

ABSTRACT

Human Metapneumovirus (hMPV) is responsible for viral respiratory infection with clinical and epidemiological relevance in pediatric, immunocompromised, and elderly populations. Little is known about hMPV *in vitro* replication processes and their relationship with cellular structures such as the cytoskeleton. Our goal was to evaluate the role of the actin cytoskeleton in hMPV replication at different stages of viral growth. hMPV was isolated in Vero cells from a clinical sample and identified as A_2 genotype. The cytopathic effect was detected by the appearance of cell rounding and refractory cell clusters. The growth curve showed that viral replication maximum level was between 48 and 72 hpi. The highest percentage of infected cells and intracellular hMPV-protein were detected at the early stages of the replication cycle. Disruption of actin microfilaments with Cytochalasin D during the early events provoked an increase in both intracellular and extracellular viruses. We demonstrate that the early phase of the hMPV curve is crucial for viral replication; and the disruption of microfilaments during this time increments both viral protein expression and release of viruses to the extracellular space. This study contributes to elucidate wild-type hMPV growth kinetics, providing new insights on the actin cytoskeleton role in viral replication mechanisms.

Keywords.

Virus isolation; Replication cycle; Actin filaments; Cytochalasin D; Respiratory disease.

60 **BACKGROUND**

61 Two members of the *Pneumoviridae* family [1] human Metapneumovirus (hMPV) and
62 respiratory syncytial virus (RSV), cause severe respiratory diseases in infants,
63 immunocompromised and older adults [2]. Currently, for RSV, a bivalent prefusion F vaccine
64 was approved for use during pregnancy in 2023 to protect infants from severe RSV illness
65 during their early months of life [3]. However, there is no licensed vaccine or approved antiviral
66 therapy available for hMPV.

67 HMPV is an enveloped negative-stranded RNA virus with a non-segmented genome composed
68 of eight genes encoding for nine proteins [4]. Two major hMPV subtypes have been described:
69 A (A1, A2a, A2b1, A2b2) and B (B1, B2) [2,5].

70 Since the discovery of hMPV [5], several approaches for its *in vitro* isolation have been
71 followed. Viral adaptation and spread in cell cultures are difficult since both require high viral
72 loads and successive blind passages of about 14-21 days to visualize the cytopathic effect
73 (CPE), characterized by changes in cell morphology or by the formation of syncytia [6,7].

74 The viral infection cycle begins with the entry of particles into susceptible cells through the
75 interaction with receptors that trigger the internalization process. Several studies have reported
76 an important role for the cytoskeleton, particularly actin microfilaments (MFLs) dynamics, in
77 entry and replication of numerous viruses, including hMPV, into the host cell [8]. In this sense,
78 it has been shown that MFLs are essential cofactors for RSV replication, spread, and
79 morphogenesis [9]. Moreover, previous studies from our laboratory demonstrated that the
80 disruption of MFLs during early stage of Pixuna virus (PIXV) replication, increased the
81 extracellular viral yields, probably promoting endocytosis and thus increasing the entry of viral
82 particles [10].

83 Despite hMPV's importance as an etiological agent of respiratory pathologies, the mechanisms
84 of interaction between virus and host cell to secure infection remain largely unexplored. We
85 examined the role of MFLs in hMPV replication at different stages of viral growth. To this end,
86 we isolated and identified hMPV circulating in Cordoba, Argentina. Furthermore, we describe
87 the hMPV replication curve and characterize the subcellular expression of viral proteins at
88 different times after infection. We demonstrate that actin depolymerization at the early phase
89 of the hMPV replication curve is crucial for a successful replication. The presence of
90 Cytochalasin D (CytD) during this period increased viral protein expression in the cytoplasm
91 and the release of viruses to the extracellular space.

92 Considering that hMPV causes a severe disease, identifying the molecular mechanisms
93 underlying its replication cycle broadens our understanding of the cell biology of viral infection.
94 Moreover, it provides possible targets to develop new antiviral treatments.

95

96 **METHODS**

97 **Cell culture and Virus isolation**

98 Vero cells (ATCC® CCL-81) were grown in Minimum Essential Medium (MEM, GIBCO-
99 BRL®) with 5-10% fetal bovine serum (FBS, Natocor), 1% antibiotic-antimycotic (Pen-Strept
100 100X, GIBCO), at 37°C and 5% CO_2.

101 Human Metapneumovirus was isolated from nasopharyngeal aspirates (NPA) of hospitalized
102 children in Cordoba, Argentina. All procedures were complied with the principles outlined by
103 the Declaration of Helsinki and were approved by an Independent Ethics Committee of Hospital
104 de Niños "Santísima Trinidad" (CIEIS) Protocol: 05/2011. The volunteers who offered samples,
105 signed written assent/consent and their personal data was kept anonymous. The infection
106 protocol was adapted from Van den Hoogen [5]. As infection medium: 0.00125% trypsin

107 (Trypsin Solution 10X, SIGMA®), 0.3% bovine serum albumin (BSA, SIGMA®) and 1%
108 antibiotic-antimycotic. The NPA positive was diluted in 2 ml of MEM without FBS and
109 centrifuged at 200*Xg* for 5 min (HSR Centrifuge Eppendorf Presvac) (NPA supernatant). Viral
110 inoculum consisted of 150 µl of NPA supernatant plus 50 µl of infection medium. Vero cells
111 (70-80% confluence) were grown in a 24-well plate with MEM. 24 hours later, the plate was
112 washed three times with PBS, 200 µl of the viral inoculum was added in each well and
113 centrifuged at 800*Xg* for 15 min (IEC International Refrigerated Centrifuge Model-PR-2).
114 Afterwards, the plate was incubated at 37°C and 5% CO_2 for 2 hours, the monolayers were
115 washed three times with PBS and 1 ml of infection medium per well was added. The infection
116 medium was changed at 4, 7, 10, 14, 17, and 21 days post-infection (dpi) and the culture
117 supernatants were stored until processed at -70°C. Cultures were observed daily for CPE by
118 phase-contrast microscopy. Three blind passages for 21 days each were performed. The hMPV
119 positive culture supernatants were used as an infection inoculum.
120
121 **RT-PCR**
122 Viral RNA was extracted from 140 µl of culture supernatants using the QIAamp® Viral RNA
123 Mini Kit (Qiagen, GmbH, Hilden, Germany) following the manufacturer's instructions. RT-
124 PCR, adapted from Bouscambert-Duchamp [11], was carried out as described by Rodriguez
125 [12].
126
127 **Indirect immunofluorescence**
128 Infected cells were grown at 60% confluence on glass coverslips during 24 hours. At different
129 times post-infection, cells were washed three times with PBS, fixed with 4% paraformaldehyde
130 and 120 mM sucrose (Sigma-Aldrich Laborchemikalien GmbH, Germany) for 20 min at room
131 temperature (RT). Immunofluorescence (IF) was performed according to Gil [10]. Cells were

132 incubated overnight with mouse anti-F protein/hMPV primary antibody (1/500) (IMAGEN™
133 hMPV. Oxoid-Ltd.) in 1% BSA/PBS at 4°C. After washed, samples were incubated with goat
134 anti-mouse secondary antibody Alexa-Fluor 488 (1/1600) (Thermo Fisher Scientific Inc., USA)
135 for 1 hour at RT. To visualize the actin filaments and nuclei, cells were labeled with Phalloidin-
136 Tetramethyl rhodamine-B (1/1000) (Sigma-Aldrich) for 1 hour at RT and Hoechst (1X) for 5
137 min. Then, samples were washed and mounted using Fluorsave (Calbiochem).
138

139 **Sequence and phylogenetic analysis**

140 The RT-PCR protocol, adaptaded from Van den Hoogen [13] to amplify a 696 bp fragment of
141 the F gene, was carried out as described by Rodriguez [12]. PCR product was purified with
142 QIAquick Gel Extraction Kit (Qiagen, Germany) following the manufacturer's instructions.
143 Nucleotide sequencing reactions were performed in both directions using the internal PCR
144 primers by Macrogen, Inc. (Seoul, Korea). Sequences were edited with MEGA-4.0.2 and
145 aligned with sequences available in the GenBank, using the ClustalW. A Maximum Likelihood
146 Tree, based on the amplified region of the fusion protein (F) gene, was generated using PhyML
147 3.0 software (Université de Montpellier, France). Branch support was evaluated via non-
148 parametric bootstrapping with 1000 pseudoreplicates. The nucleotide substitution model was
149 choosen based on the AIC implemented in ModelTest-3.7 software (University of Vigo, Spain).
150 The sequence was deposited in GenBank (accession no. **MN117139**).
151

152 **Viral quantification by RT-qPCR**

153 Viral RNA copies from different supernatants were determined by absolute quantification in an
154 Applied Biosystems 7500 Fast-Real-time PCR system. The reaction mix was prepared by
155 adapting the manufacturer's protocol for AgPath-ID™ One-Step RT-PCR Reagents (Applied
156 Biosystems™): 2X RT-PCR Buffer= 1X; Forward and reverse PCR primers= 50µM each;

157 Syber Green (SYBR™ Green 10000X-Invitrogen) dilution 1/100= 5.0 and -5; 25X RT-PCR
158 Enzyme Mix (ArrayScript™ Reverse Transcriptase and AmpliTaq Gold®DNA Polymerase)=
159 1X. The final volume was 25 µl, using 2.5 µl of viral RNA. Cycling conditions: 50°C for 30
160 min; 45 cycles of 94°C for 2 min 95°C for 10 sec, 60°C for 30 sec and 72°C for 30 sec and a
161 final step of 72°C for 10 min. Data were analyzed in real-time using the Virtual Curve qPCR
162 program from Applied Biosystems (Thermo Fisher Connect™). Viral load was calculated from
163 a standard curve generated with serial dilutions (10^{-1} to 10^{-12}) of an hMPV N protein synthetic
164 oligonucleotide (199 bp) (Ultramer® DNA Oligo) with a known concentration (6.0219×10^{13}
165 copies of RNA/µl).

166

167 **hMPV Replication Curve**

168 Vero cells were grown (60% confluence) on glass coverslips (12mm in 24-well plate) for 24
169 hours and then infected with isolated hMPV (1.97×10^{6} copies of RNA/µl). The culture
170 supernatants were harvested and the monolayers were fixed at different time points (8, 16, 24,
171 48, 72, and 96 hpi). Viral RNA was extracted from harvested supernatants, then the extracted
172 RNA was employed for the detection and quantification of hMPV. The mean number of copies
173 of extracellular viral RNA/µl of culture supernatant was then calculated (Applied biosystems.
174 Thermo-Fisher-Connect™).
175 Cells were processed for IF and the number of fluorescent dots/infected cell were calculated
176 through the analysis of fluorescence images using the ImageJ-Fiji software (ImageJ 1.50c
177 Wayne Rasband. NIH-USA).

178

179 **Pharmacological treatment**

180 Vero cells at 60% confluence cultured on glass coverslips were infected with hMPV. Infected
181 cells treated with CytD [2.5µM] [10] or vehicle (infection medium whitout CytD) were analized

182 at different times during the replication cycle. Cells were exposed to CytD or vehicle during
183 the 2 infection hours, as well as throughout the first 8 hpi (experimental period between 0-24
184 hpi); during the first and the last 24 hours (48-72 hpi) in an experimental period between 0-72
185 hpi. In each case, the supernatant was removed, the cells were washed three times with PBS
186 and the infection medium was added according to each treatment (Fig. 3B). Culture
187 supernatants and harvested cells were processed for RNA extraction, viral quantification by
188 RT-qPCR and IF, respectively.
189
190 **Microscopy and digital image analysis**
191 Immunostained cells were visualized using an inverted epi-fluorescence microscope (Olympus
192 IX81, Olympus). Images were taken with a regular fluorescence microscopy with a CCD
193 camera (Orca 1000, Hamamatsu-Corp.) and with an inverted confocal microscope FV1000
194 (Olympus). The collection and processing of data from the images were analyzed with the
195 ImageJ-Fiji software. Quantification of intracellular infection was carried out by the percentage
196 of infected cells and the number of fluorescent dots/ infected cell.
197
198 **Statistical analysis**
199 All tests and graphs were performed using GraphPad Prism 8.0 (GraphPad Software). Data
200 represent results from at least three independent experiments, and values are presented as the
201 mean ± standard error of the mean (SEM). Assumptions of homoscedasticity and normality
202 were tested using Brown-Forsythe and Barlett´s tests and D´Agostino & Pearson test,
203 respectively. All assumptions were met, allowing the use of Student's unpaired t-test or one-
204 way ANOVA test for specific group comparisons. A significance level of $p < 0.05$ was
205 considered statistically significant.
206

207 **RESULTS**

208 **Human-Metapneumovirus isolation and identification**

209 Human Metapneumovirus was isolated from NPA of hospitalized children in Cordoba,
210 Argentina.

211 The virus replicated in Vero cells cultures after three blind passages of 21 days each one. The
212 CPE was characterized by cell rounding, detachment, and formation of refractory cell clusters
213 (Fig. 1A). IF detection confirmed that the CPE was caused by hMPV. The presence of specific
214 hMPV proteins was observed at 4, 7, and 14 dpi located and distributed in the cell cytoplasm
215 presenting a dotted pattern (Fig. 1B). Simultaneously, virus genome detection by nucleic acid
216 amplification assays (RT-PCR) from supernatants of infected cultures collected at 4, 7, and 14
217 dpi were positive for the amplification of the 199 bp N protein (Fig. 1C), confirming the
218 presence of hMPV in infected culture. Viral isolation was typified, the
219 Cordoba/ARG/3864/2015 local isolated strain (no: MN117139) was identified as A_2 hMPV and
220 grouped with Canada and The Netherlands prototype strains, and with sequences from
221 Argentina [12,14], Peru, Brazil, United States, China, and Italy (Fig. 1F).

222 Different subcellular localization of large fluorescent dots were observed several times post-
223 infection (Fig. 1B and D), while confocal microscopy detected small dots between 0 and 96 hpi
224 in the subcortical area enriched in actin filaments, below the plasma membrane (Fig. 1E, low
225 panel).

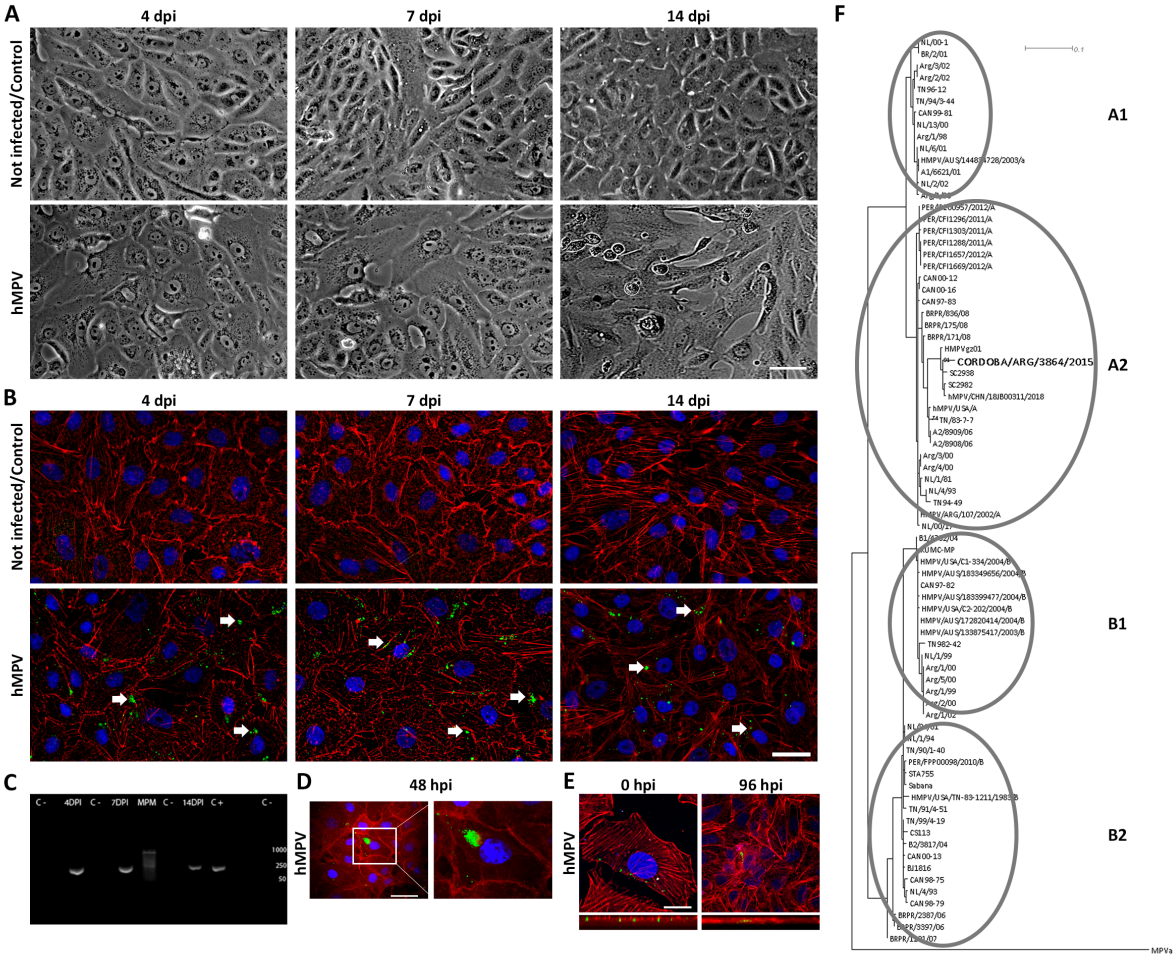

Figure 1. Human Metapneumovirus (hMPV) isolation and identification. A and B: Representative images of uninfected and infected VERO cells with hMPV. **A-** Images were obtained with phase contrast microscopy at low magnification, showing the viral infection cytopathic effect (CPE), which is visible at 14 d.p.i as cell rounding and shedding. Uninfected cells (top panel) and infected cells (bottom panel) at 4, 7 and 14 days dpi. Scale bar: 20 µm. **B-** The localization of the hMPV protein was determined using indirect immunofluorescence with specific anti-hMPV antibodies targeting protein F (green). MFLs were labeled with Phalloidin-Rho (red), and nuclei were stained with Hoechst (blue). A temporary sequence of 4 to 14 days in non infected (top panel) and infected cells (bottom panel). White arrows indicate the fluorescent label of the F protein. Scale bar: 20 µm. **C-** Amplification products (RT-PCR) of the hMPV N protein region (199 bp) by agarose gel electrophoresis. Bands corresponding to culture supernatants of infected cells collected at 4, 7 and 14 dpi and positive controls (C+) are shown. Uninfected cells collected at the same times are included (C-). MPM: molecular weight marker. **D-** Images obtained with epi-fluorescence microscopy, showing that the hMPV F protein accumulates near the nucleus at 48 hpi. Scale bar: 100 µm. **E-** Confocal microscopy images where viral proteins are observed at 0 and 96 hpi. The bottom panel shows a transverse optical section where the viral label is evidenced in the cell cytoplasm decorating the MFLs. Scale bar: 20 µm. **F-** A maximum-likelihood tree (PhyML software) was constructed, using the GTR+G model with parameters suggested by JModelTest 3.7 with bootstraps and 1000 pseudoreplicates. A1: strains to hMPV subgroup A1. A2: strains to hMPV subgroup A2. B1: strains to hMPV subgroup B1. B2: strains to hMPV subgroup B2. Avian MPV (aMPV) was

248 used to root the tree. The strain of interest is marked in bold. The scale bar indicates the changes
249 between nucleotides. All data were obteinded from 5 independet experiments.

250

251 **The hMPV replication cycle**

252 To characterize hMPV replication kinetics, we evaluated the production and release of the virus
253 over time (8, 16, 24, 48, 72, and 96 hpi) using qRT-PCR (RNA copies/µl of culture
254 supernatant). RNA copies increased progressively until 72 hpi, peaking at 4,961 copies/µl of
255 supernatant (Fig. 2A). The time course of hMPV infection was also studied by IF and viral
256 proteins was quantified as number of fluorescent dots/infected cell (Fig. 2B and D).
257 Interestingly, the number of fluorescent dots/infected cell decreased while the number of copies
258 of RNA/µl of culture supernatant increased. At 72 hpi the maximum extracellular viral yield
259 (4,961 copies) corresponded to the minimum number of cytoplasmic dots (2.2 dots), as well as
260 to the lowest percentage of infected cells (32.8%) (Fig. 2C). It is important to highlight that the
261 percentage of infected cells decreased significantly and progressively from 24 hpi until the end
262 of the experiment (Fig. 2C and D).

263 Taken together, our results demonstrate that the highest percentage of infected cells and
264 intracellular hMPV-protein contents were detected at the early phase of the replication cycle.
265 While the cycle progressed, hMPV immunostaining decreased whereas extracellular viral RNA
266 increased due to the release of the viral progeny.

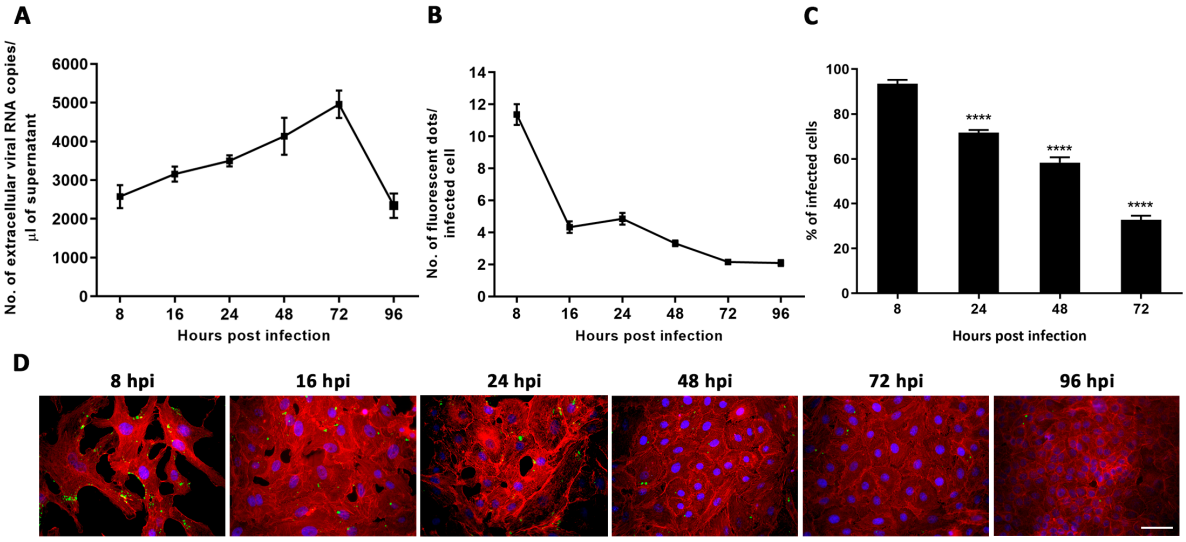

Figure 2. HMPV viral replication curve. A- Quantification curve of extracellular viral production through the number of copies of viral RNA in the extracellular medium. Quantification was performed at 8, 16, 24, 48, 72 and 96 hpi. **B-** Quantification of intracellular viral production through the number of fluorescent dots/infected cell (cytoplasmic viral F protein). Quantification was performed at 8, 16, 24, 48, 72 and 96 hpi **C-** Percentage of quantified infected cells was determined by the number of cells with or without fluorescent dots at 8, 24, 48, and 72 hpi. **D-** Representative images of the temporal sequence of infection (0-96 hpi). The hMPV F protein label (green), MFLs (red) and nuclei (Hoechst, blue) are observed. Scale bar: 20 µm. More than 400 cells were screened in each time point. Data represent the mean ± SEM from 3 independent experiments (one-way ANOVA with Tukey test post hoc test). **** <0.0001.

Actin microfilament perturbation at different viral stages affects hMPV replication.

Previous studies highlight the involvement of the cytoskeleton, particularly MFLs, in the entry and replication of numerous viruses [8]. Therefore, we studied the role of MFLs at early and late stages of hMPV infection cycle. For this, disruption of actin polymerization was performed using CytD at different times of hMPV infection. We first determined the participation of MFLs during the entry and at its early stages of hMPV replication. To this end, CytD was applied during virus infection (2 hours), during the first 8 hpi and during the first 24 hpi (Fig. 3B). Treatment with CytD during early replication stages prevented the significant decrease in the number of infected cells, maintaining initial percentage, regardless of drug exposure timing (Fig. 3A and C). Interestingly, CytD treatment during the first 24 hpi, also prevented the

290 dramatic diminution in the percentage of infected cells at 72 hpi (75.3%) compared to control
291 (33.3%) (Fig. 3C). To obtain a quantitative measure of CytD effect on F viral protein expression
292 at the different stages of the replication cycle, we quantified the number of fluorescent
293 dots/infected cell. CytD treatment during infection or during the first 8 hpi significantly
294 increased fluorescent dots/infected cell compared to controls (Fig. 3A and D). Particularly,
295 during the first 8 hpi of treatment a 2 to 2.5 fold increase was observed at both analyzed times
296 (8 hpi and 24 hpi) (Fig. 3A and D). When CytD was applied during the first 24 hpi, and
297 quantified at the end of the treatment, no significant differences in fluorescent dots/infected
298 cells was observed compared to control, but prevented viral protein loss at 72 hpi (Fig. 3D).
299 Finally, we quantified viral-RNA copies in culture supernatant to assess extracellular virus
300 yields (Figure 3E). CytD treatment during the infection significantly increased viral production
301 at 24 hpi. Treatment during the first 8 hpi significantly increased RNA copies at that time. This
302 effect was also observed in the accumulated values, this value is the sum of the mean of RNA
303 copies values at 8 plus 24 hpi (for vehicle: 6,674; CytD treatment: 10,727; see accumulated
304 value at 24 hpi). On the other hand, CytD treatment during the first 24 hpi, caused a significant
305 decrease in extracellular RNA viral copies at 24 hpi, remaining lower up to 72 hpi, as can be
306 observed in the accumulated values (vehicle: 4,510; CytD treatment: 2,930; see accumulated
307 value at 72 hpi) (Fig. 3E).
308 In addition, we focused on the late stage of the replication curve and observed that CytD applied
309 during the last 24 hpi (48-72 hpi) caused no changes in the percentage of infected cells, in the
310 number of fluorescent dots/infected cell or in the number of extracellular RNA-viral copies
311 compared to controls (data not shown).
312 These results underscore the importance of the initial 8 hours of hMPV infection for replication,
313 indicating that CytD presence during this period boots viral protein expression in the cell
314 cytoplasm and enhances virus release into extracellular space.

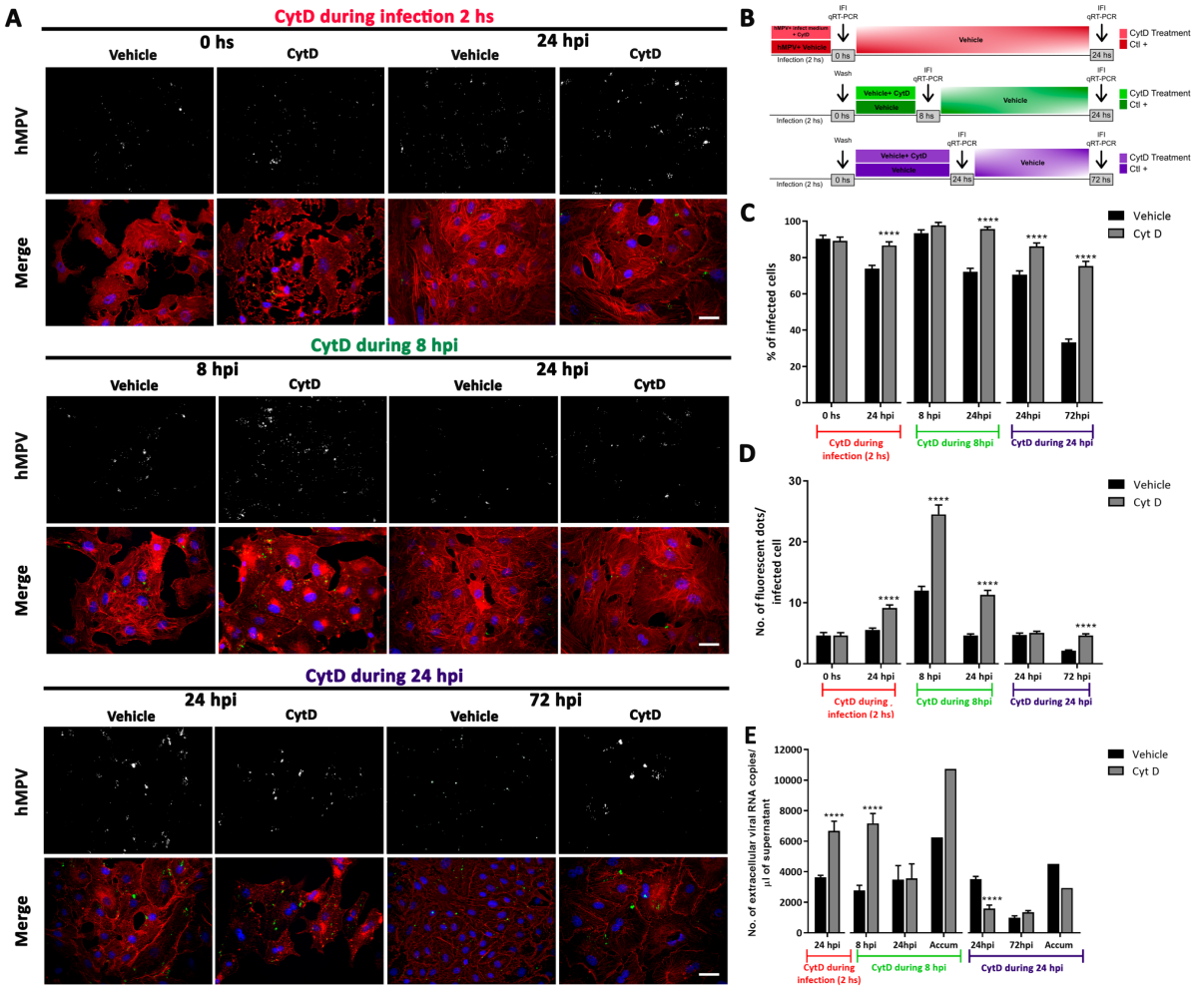

Figure 3. Effect of disruption of MFLs with CytD at different stages of the viral cycle. A- Images of CytD treatments in hMPV infected cells at different times of the growth curve: CytD during infection (2 h), during 8 hpi and during 24 hpi. Immunofluorescence performed with specific hMPV antibodies anti-protein F (green), MFLs (Phalloidin-Rho, red) and nuclei (Hoechst, blue). **B-** The scheme illustrates the pharmacological treatment with CytD at different times during the viral replication cycle and the time points of experimental procedures. In red color: cells exposed to vehicle or CytD during the 2 infection hours. In green color: cells exposed to vehicle or CytD throughout the first 8 hpi. In violet color: cells exposed to vehicle or CytD during the first 24 hpi. **C-** Percentage of infected cells after CytD treatment in relation to vehicle control. CytD treatment during infection (2 h): a significant increase was observed at 24 hpi ($p < 0.0001$). CytD treatment during the first 8 hpi: a significant increase was observed at 24 hpi ($p<0.0001$). In CytD treatment during first 24 hpi a significant increase was observed both at 24 and 72 hpi (24 hpi: $p<0.0001$; 72 hpi: $p<0.0001$). **D-** Number of fluorescent dots per infected cell in CytD treatments and in controls. CytD treatment during infection (2 h): a significant increase was observed at 24 hpi ($p < 0.0001$). CytD treatment during the first 8 hpi: a significant increase was observed both at 8 and 24 hpi (8 hpi: $p < 0.0001$; 24 hpi: $p < 0.0001$). CytD treatment during the first 24 hpi: a significant increase was observed at 72 hpi ($p<0.0001$). **E-** Quantification of extracellular viral RNA. CytD treatment during infection (2 h): a significant increase in RNA copies in the culture supernatant was observed at 24 hpi ($p<0.0001$). CytD treatment during the first 8 hpi caused a significant increase in RNA copies in culture supernatant at 8 hpi ($p<0.0001$); this was also observed in the accumulated values

(sum of the means of RNA copies at 8 plus 24 hpi). CytD treatment during the first 24 hpi caused a significant decrease in extracellular viral RNA copies ($p < 0.0001$), remaining constant until 72 hpi; this was also observed in the accumulated values (sum of the means of RNA copies at 24 and 72 hpi). Scale bar: 20 µm. More than 400 cells were screened in each case. Data represent the mean ± SEM from 3 independent experiments. Student unpaired *t* test was performed (**** <0.0001).

DISCUSSION

In this study we report the first successful isolation of hMPV performed in Vero cell line from a positive clinical sample in Cordoba, Argentina. We identified this local strain and described the replication curve showing that the maximum viral production takes place at 72 hpi. Moreover, we demonstrate that the disruption of MFL at the early stages of infection increases intracellular viral production and the release of viruses into the extracellular space.

The viral isolate was identified as the A_2 hMPV subtype through phylogenetic analysis, consistent with our previous studies of A_2 hMPV subtype circulation in Argentina [12]. Additionally, co-circulation with other genotypes like A_1, B_1, and B_2, has been reported in our country [14]. Genotype predominance varies based on factors like epidemiological year and region, host immunity, viral load, and susceptibility. Competitive replication was observed between hMPV genotype A and B. A recent study by van den Hoogen's group [15] demonstrated that lineage A replicates more efficiently than lineage B in an organoid-derived human bronchial-epithelium model, with increased viral-RNA and infectious virus particles. They also highlight the use of viruses with a history of controlled passage, instead of extensively passaged hMPV strains. These data are important because the A_2 genotype is clinically relevant, as it may cause diseases of varying severity. In studies where verification was possible, genotype A has been associated with severe conditions such as pneumonia and hypoxia, leading to more ICU admissions compared to the other subtypes [16].

In several studies, hMPV replication is limited to certain cell lines, with varied and mild CPE. Isolation of the A_2 hMPV viral strain in this study showed initial CPE signs at the third blind

365 passage, at 14 dpi, characterized by cell rounding and refractive cells clusters, consistent with
366 previous reports [7,17]. Conversely, other authors have described that hMPV can appear as a
367 syncytium [5,6,18], similar to RSV, and this difference may be related to the cell lines that were
368 infected (e.g. LLC-MK2, tMK, MNT-1, A549) or to the viral genotype [19–21]. Numerous
369 authors note the challenge of hMPV isolation and the absence of an obvious CPE [5,19,20,22].
370 Isolating respiratory viruses from clinical specimens often exhibits low efficiency *in vitro* due
371 to factors like cell type and virus subtype [17,22–24]. LLC-MK2 and Vero cells are commonly
372 used for all hMPV strains. Although, this study did not compare different cell lines and isolated
373 only the A2 hMPV subtype, efficient viral replication was achieved, consistent with findings
374 by Nao [21] who demonstrated high infectivity with different hMPV strains in VeroE6 and
375 Vero-ATCC cells.

376 The hMPV replication curve showed an exponential phase between 48 to 72 hpi, with maximum
377 intracellular viral protein concentration at 8 hpi which is consistent with results obtained by
378 other groups. Tollefson et al. [19] described hMPV kinetics in LLC-MK2 cells, with the eclipse
379 phase at 24 hpi and the exponential phase between 48 and 72 hpi with a significant increase in
380 viral titer. El Najjar [25] showed maximum viral production at 72 hpi in BEAS-2B cells, both
381 intra- and extracellularly. Recent studies using recombinant viruses in Vero cells, three-
382 dimensional cultures and organoid-derived bronchial culture have described similar results,
383 both in the CPE caused by the virus and in the replicative cycle [15,16,26]. All these results
384 show that our model of infection in the Vero-CCL cell line with this wild-type virus (A_2 hMPV),
385 despite its isolation difficulties, is very efficient and representative of *in vivo* infection.

386 It is known that viruses such as RSV [9] and PIXV [10], among others, take advantage of
387 structures such as the cytoskeleton for entry, replication and exit from the cell. Our study aimed
388 to assess the role of actin cytoskeleton in hMPV replication. For this, we used CytD, known to
389 disrupt actin polymerization. CytD concentration [2.5μM] was effective and consistent with

390 prior studies [24,25] as well as previously in our laboratory with another viral model [10]. The
391 rapid reversible action of CytD facilitated our experimental designs. Intracellularly, CytD not
392 only prevented the decrease in the percentage of hMPV-infected cells (during 2 hours of
393 infection, 8 hpi and 24 hpi) but it also caused a significant increase in the number of fluorescent
394 dots/infected cell, indicative of protein accumulations, in all treatments. In line with this, El
395 Najjar [25] postulates that hMPV proteins assembly during early infection does not require
396 actin polymerization. These protein accumulations (fluorescent dots), resembling "inclusion
397 bodies" [27,28] persist despite actin alteration, hindering viral release. Cifuentes-Muñoz [24]
398 note these structures as primary replication sites, particulary at 24 hpi. In *Pneumovirus*, actin
399 polymerization partially aids inclusion body formation [17]. Unlike Cifuentes-Muñoz [24], our
400 early CytD treatment (8 hpi) boosts extracellular viral load, suggesting that MFLs interruption
401 could facilitate viral entry. This represents an increase in intracellular viral load and a decrease
402 in virus release times, compared to the control. Nevertheless, our results are consistent with
403 those of Cifuentes-Muñoz [24] and El Najjar [25] regarding reduced extracellular viral load
404 from 24 hpi, particularly with continuous 24-hour treatment. Several studies suggest that hMPV
405 relies on cell-cell transmission for efficient spread and infection [8,28–30]. Actin disruption
406 may hinder this process, redirecting virions to alternate exit routes and leading to extracellular
407 accumulation. Therefore, actin dynamics is essential for hMPV infection, enabling cell-to-cell
408 spread regardless of the extracellular viral load [25]. This could explain cytoplasmic viral
409 protein accumulation and the decrease of extracellular viral load after 24 hpi CytD exposure.
410 Given MFLs are involved in viral particle internalization and release [24], it is reasonable to
411 think that short-term disruption of MFLs with CytD would facilitate viral particles
412 internalization. Conversely, prolonged CytD treatment (24 hpi), could prevent the transport of
413 viral proteins and/or nucleocapsid, reducing cytoplasmic accumulation and extracellular viral
414 loading. Despite the years since its discovery, the cell biology of hMPV infection remains

415 poorly understood. This study broadens our knowledge on the isolation and growth curve
416 characterization of a wild-type hMPV obtained from a clinical sample. Furthermore, these
417 findings provide new insights on hMPV infection and the role of actin cytoskeleton in viral
418 replication, enhancing understanding of hMPV internalization and spreading mechanisms.

419

420 **ACKNOWLEDGEMENTS**

421 We would like to thank Bernadette van den Hoogen for receiving PER in her laboratory and for
422 advising on the viral isolation protocol; Guadalupe Carballal† and Cristina Videla for
423 generously providing hMPV wild type positive control; Celia Frutos and Lucia Ghietto for
424 technical assistance in Real Time RT-qPCR; Santiago Mirazo for generously providing
425 polyclonal antibodies; Carlos Mas for technical assistance in confocal microscopy at the Centro
426 de Micro y Nanoscopía de Córdoba, CEMINCO-CONICET-Universidad Nacional de Córdoba,
427 Córdoba, Argentina. We particularly want to thank Miss Stella Ascheri for general technical
428 assistance.

429

430 **DATA AVAILABILITY STATEMENT**

431 The data that support the findings of this study are available from the corresponding author
432 [gpaglini@immf.uncor.edu] upon reasonable request.

433

434 **DECLARATIONS**

435 **Conflict of Interest.** The authors have no competing interests to declare that are relevant to the
436 content of this article.

Funding source. This work was supported by grants from Secretaria de Ciencia y Tecnología-Universidad Nacional de Córdoba (SECYT-Consolidar-I Nº 336 20180100191CB to A.C. and SECYT-Consolidar-C Nº 33620180100091CB to M.G.P.) and from Fundación A. J. Roemmers (2018-2020 to A.C. and 2017-2019 to P.E.R). The funding sources had no involvement in the study design, data collection, analysis and interpretation, writing of the manuscript or in the decision to submit the article for publication.

REFERENCES

1. Afonso CL, Gaya KA, Bányai K, et al.: TAXONOMY OF THE ORDER MONONEGAVIRALES: UPDATE 2016. Arch Virol **2016**; 161:2351–2360.
2. Shafagati N, Williams J: Human metapneumovirus - what we know now. F1000Research **2018**; 7:1–11.
3. Kampmann B, Madhi SA, Munjal I, et al.: Bivalent Prefusion F Vaccine in Pregnancy to Prevent RSV Illness in Infants. N Engl J Med **2023**; 388:1451–1464.
4. Ballegeer M, Saelens X: Cell-Mediated Responses to Human Metapneumovirus Infection. Viruses **2020**; 12:3–22.
5. Van Den Hoogen BG, De Jong JC, Groen J, et al.: A newly discovered human pneumovirus isolated from young children with respiratory tract disease. Nat Med **2001**; 7:719–724.
6. Sato K, Watanabe O, Ohmiya S, et al.: Efficient isolation of human metapneumovirus using MNT-1, a human malignant melanoma cell line with early and distinct cytopathic effects. Microbiol Immunol **2017**; 61:497–506.
7. Deffrasnes C, Côté S, Boivin G: Analysis of Replication Kinetics of the Human Metapneumovirus in Different Cell Lines by Real-Time PCR. J Clin Microbiol **2005**; 43:488–490.

462 8. Cifuentes-Munoz N, El Najjar F, Dutch RE: Viral cell-to-cell spread: Conventional and
463 non-conventional ways. In: Advances in Virus Research. **2020**. p. 85–125.
464 9. Shahriari S, Wei KJ, Ghildyal R: Respiratory syncytial virus matrix (M) protein
465 interacts with actin in vitro and in cell culture. Viruses **2018**; 10:7–12.
466 10. Gil PI, Albrieu-Llinás G, Mlewski EC, et al.: Pixuna virus modifies host cell
467 cytoskeleton to secure infection. Sci Rep **2017**; 7:1–9.
468 11. Bouscambert-Duchamp M, Lina B, Trompette A, Moret H, Motte J, Andréoletti L:
469 Detection of human metapneumovirus RNA sequences in nasopharyngeal aspirates of
470 young french children with acute bronchiolitis by real-time reverse transcriptase PCR
471 and phylogenetic analysis. J Clin Microbiol **2005**; 43:1411–1414.
472 12. Rodriguez PE, Frutos MC, Adamo MP, et al.: Human Metapneumovirus:
473 Epidemiology and genotype diversity in children and adult patients with respiratory
474 infection in Córdoba, Argentina. PLoS One **2020**; 15:e0244093.
475 13. Van Den Hoogen BG, Osterhaus DME, Fouchier RAM: Clinical impact and diagnosis
476 of human metapneumovirus infection. Pediatr Infect Dis J **2004**; 23:25–32.
477 14. Velez Rueda AJ, Mistchenko AS, Viegas M: Phylogenetic and Phylodynamic Analyses
478 of Human Metapneumovirus in Buenos Aires (Argentina) for a Three-Year Period
479 (2009-2011). PLoS One **2013**; 8:1–10.
480 15. Ribó-Molina P, van Nieuwkoop S, Mykytyn AZ, et al.: Human metapneumovirus
481 infection of organoid-derived human bronchial epithelium represents cell tropism and
482 cytopathology as observed in in vivo models. Virology **2024**; 9:1–13.
483 16. Arnott A, Vong S, Sek M, et al.: Genetic variability of human metapneumovirus
484 amongst an all ages population in Cambodia between 2007 and 2009. Infect Genet
485 Evol **2013**; 15:43–52.
486 17. Kinder JT, Moncman CL, Barrett C, Jin H, Kallewaard N, Dutch RE: Respiratory

487 Syncytial Virus and Human Metapneumovirus Infections in Three-Dimensional
488 Human Airway Tissues Expose an Interesting Dichotomy in Viral Replication, Spread,
489 and Inhibition by Neutralizing Antibodies. J Virol **2020**; 94:1–20.
490 18. Bernal LJ, Velandia-Romero M, Guevara C, Castellanos JE: Human
491 Metapneumovirus: Laboratory Methods for Isolation, Propagation, and Plaque
492 Titration. Intervirology **2019**; 61:301–306.
493 19. Tollefson SJ, Cox RG, Williams J V: Studies of culture conditions and environmental
494 stability of human metapneumovirus. Virus Res **2010**; 151:54–59.
495 20. Jumat MR, Nguyen Huong T, Wong P, et al.: Imaging analysis of human
496 metapneumovirus-infected cells provides evidence for the involvement of F-actin and
497 the raft-lipid microdomains in virus morphogenesis. Virol J **2014**; 11:1–12.
498 21. Nao N, Sato K, Yamagishi J, et al.: Consensus and variations in cell line specificity
499 among human metapneumovirus strains. PLoS One **2019**; 14:1–21.
500 22. Lee H, Woo HM, Kim K, et al.: Improving pneumovirus isolation using a
501 centrifugation and AZD1480 combined method. J Microbiol Biotechnol **2019**;
502 29:2006–2013.
503 23. Cox RG, Mainou BA, Johnson M, et al.: Human Metapneumovirus Is Capable of
504 Entering Cells by Fusion with Endosomal Membranes. PLoS Pathog **2015**; 11:1–29.
505 24. Cifuentes-muñoz N, Branttie J, Slaughter KB, Dutch RE: Human Metapneumovirus
506 Induces Formation of Inclusion Bodies for Efficient Genome Replication and
507 Transcription. J Virol **2017**; 91:1–18.
508 25. El Najjar F, Cifuentes-Muñoz N, Chen J, et al.: Human metapneumovirus Induces
509 Reorganization of the Actin Cytoskeleton for Direct Cell-to-Cell Spread. PLoS Pathog
510 **2016**; 12:1–30.
511 26. Geiser J, Boivin G, Huang S, et al.: RSV and HMPV Infections in 3D Tissue Cultures:

512 Mechanisms Involved in Virus-Host and Virus-Virus Interactions. Viruses **2021**; 13:1–
513 15.
514 27. Derdowski A, Peters TR, Glover N, et al.: Human metapneumovirus nucleoprotein and
515 phosphoprotein interact and provide the minimal requirements for inclusion body
516 formation. J Gen Virol **2008**; 89:2698–2708.
517 28. Najjar F El, Castillo SR, Moncman CL, et al.: Imaging analysis reveals budding of
518 filamentous human metapneumovirus virions and direct transfer of inclusion bodies
519 through intercellular extensions. MBio **2023**; 14:1–18.
520 29. Merwaiss F, Czibener C, Alvarez DE: Cell-to-cell transmission is the main mechanism
521 supporting bovine viral diarrhea virus spread in cell culture. J Virol **2018**; 93:1–18.
522 30. Boggs KB, Edmonds K, Cifuentes-Munoz N, et al.: Human Metapneumovirus
523 Phosphoprotein Independently Drives Phase Separation and Recruits Nucleoprotein to
524 Liquid-Like Bodies. MBio **2022**; 13:.
525